Rare Met. (2021) 40(10):2956–2963
https://doi.org/10.1007/s12598-020-01661-5

RARE METALS

ORIGINAL ARTICLE

Microstructure and mechanical properties of high-strength high-pressure die-cast Mg–4Al–3La–1Ca–0.3Mn alloy

Peng-Fei Qin, Qiang Yang*, Yu-Ying He, Jing-Huai Zhang*, Jin-Shu Xie, Xi-Ru Hua, Kai Guan, Jian Meng

Received: 18 August 2020 / Revised: 16 September 2020 / Accepted: 21 September 2020 / Published online: 19 January 2021

Abstract A new high-pressure die-cast (HPDC) Mg–4Al–3La–1Ca–0.3Mn (ALaX431) alloy with high strength has successfully been fabricated. This HPDC alloy in peak-aged state exhibits tensile yield strength (TYS) of 220 MPa at room temperature and TYS of 145 MPa at 250 °C, higher than the corresponding strength of HPDC Mg alloys reported so far. These high strengths are mainly due to the formation of fine grained structure, semi-continuous reticular structure consisting of stable Al_3La and $(Mg,Al)_2Ca$ particles along grain boundaries and numerous nanoscale Al_2Ca precipitates within grains. Due to its higher strength than existing HPDC Mg alloys, the new developed alloy has great application potential.

Keywords Magnesium alloys; High-pressure die-cast; Mechanical property; Intermetallic phase

P.-F. Qin, Y.-Y. He, J.-H. Zhang*, J.-S. Xie, X.-R. Hua
Key Laboratory of Superlight Materials and Surface Technology, Ministry of Education, Harbin Engineering University, Harbin 150001, China
e-mail: zhangjinghuai@hrbeu.edu.cn

P.-F. Qin, Q. Yang*, X.-R. Hua, J. Meng
State Key Laboratory of Rare Earth Resource Utilization, Changchun Institute of Applied Chemistry, Chinese Academy of Sciences, Changchun 130022, China
e-mail: qiangyang@ciac.ac.cn

K. Guan
Department of Materials Science and Engineering, University of Tokyo, Tokyo 113-8654, Japan

1 Introduction

High-pressure die-cast (HPDC) Mg–Al–RE (RE = rare earth)-based alloys have been becoming a potential material in the automotive applications due to its light weight and acceptable comprehensive performances such as good castability, mechanical and anti-corrosion properties [1–4]. As a representative alloy in this system, AE44 (E represents Ce-rich mischmetal) alloy has been successfully applied to the engine cradle [2, 5]. Nevertheless, its strength is still far from the alloys such as high-strength Al alloys and next-generation steel. In addition, relatively high cost also limits its widespread use in industrial production. To solve the above issues, researchers have begun to focus on combination of cheap alkaline earth elements and optimized RE to develop new higher performance HPDC Mg alloys.

Related studies have shown that calcium (Ca) can enhance the strength and creep resistance of Mg–Al-based alloys under certain conditions [6–12]. For example, Yang et al. [11] reported that addition of Ca to HPDC Mg–4Al–2RE (Ce-rich mischmetal) alloy can enhance yield strength by forming strong intermetallic skeleton. Zhang et al. [12] found that the addition of Ca can effectively improve the creep resistance of the metal mold-casted Mg–4Al–1RE (Ce-rich mischmetal) alloy. On the other hand, the previous research showed that the kind of RE elements could affect the microstructures and mechanical properties of Mg alloys [13–22]. Anyanwu et al. [21] found that La addition can enhance the creep resistance of Mg–0.6Zn–6Al–1Ca alloy more effectively than Ce-rich mischmetal. More recently, Zhang et al. [13, 14, 16] and Zhu et al. [22] reported that the Mg–4Al–4La (ALa44) alloy exhibits superior strength, and creep resistance compared to the Mg–4Al–4Ce (ACe44) and Mg–4Al–4Nd (ANd44) alloys.

Based on the above analysis, it is feasible to develop new Mg–Al–La–Ca alloys with outstanding mechanical properties. Additionally, we try to apply short-term aging treatment in HPDC Mg–Al–RE-based alloys so as to further improve the alloy strength. In this paper, the microstructure and mechanical properties of a newly designed HPDC Mg–4Al–3La–1Ca–0.3Mn (ALaX431) alloy are reported. The results make-up a basis for the development of high performance HPDC Mg alloys.

2 Experimental

The Mg–4Al–3La–1Ca–0.3Mn (ALaX431) alloy was produced from pure Mg, pure Al, Mg–23 wt%La, Mg–28 wt%Ca and Mg–2 wt%Mn master alloys. The alloy was melted in an electric resistance furnace under $CO_2 + SF_6$ mixed gas protection. When the temperature reached to ~ 740 °C, the melt was stirred for ~ 10 min. After cooling to (700 ± 5) °C, the melt was poured into a die preheated to ~ 240 °C. Finally, tensile test bars with diameter of 6 mm and length of 60 mm were produced by a cold chamber die-cast machine. The chemical compositions of the obtained alloy determined by inductively coupled plasma atomic emission spectrum (ICP-AES, ICAP6300) were Mg–3.9Al–3.2La–0.84Ca–0.32Mn (wt%). Some HPDC tensile test bars were further aged at (200 ± 2) °C for various durations.

The tensile tests were performed using an Instron 5869 tensile testing machine under an initial strain rate of 1.0×10^{-3} s^{-1} at room temperature (RT, 20 °C), 150, 200 and 250 °C, respectively. The tensile data showed in this study were the average of at least four valid measurements to ensure reliability. Samples for microstructural analysis are from the middle part of the tensile bars. The microstructure of the as-cast and peak-aged alloy was characterized by optical microscope (OM, Olympus-GX71), X-ray diffraction (XRD, D/max2500PC, Bruker D8 FOCUS) with Cu Kα radiation ($\lambda = 0.15406$ nm), backscatter scanning electron microscope (SEM, Hitachi S-4800) and transmission electron microscope (TEM, FEI Tecnai G^2 F20) equipped with an energy dispersive spectrometer (EDS). Specimens for OM or SEM observation were etched in a 4% HNO_3/C_2H_5OH solution for about 15 s. Thin foils for TEM observation were prepared using a precision ion polishing system (PIPS Gatan).

3 Results and discussion

3.1 Microstructure of as-cast ALaX431 alloy

Figure 1a shows OM image of as-cast ALaX431 alloy. It is clear that the microstructure is consisted of α-Mg grains and intermetallic phases along grain boundaries. Using the line intercept method, the average grain size is measured to be (8.3 ± 0.5) μm. According to relevant literature reports [23, 24], the grain sizes of HPDC Mg–4Al–4RE (RE = Ce-rich mischmetal, Ce, La) and Mg–Al–Ca-based alloys are generally above 10 μm. It can be inferred that the co-addition of Ca and La is more effective in grain refinement of Mg–Al-based alloys than the addition of RE or Ca alone. The magnified backscatter SEM image shows that the intermetallic phases in ALaX431 alloy mainly present three morphologies, i.e., acicular, lamellar and irregular block shapes (Fig. 1b). These intermetallics with ~ 0.5–3.0 μm in length and 100–500 nm in width are mainly distributed on the grain boundaries and interconnected to form a semi-continuous reticular structure.

To confirm these intermetallic phases formed in as-cast ALaX431 alloy, phase morphology and structure were further characterized by TEM. Figure 2a–c shows respectively the bright-field TEM (BF-TEM) image, the corresponding selected area electron diffraction (SAED) pattern and EDS analysis result of phase with acicular shape. SAED pattern is highly consistent with that of Al_3La phase reported previously [25]. EDS analysis indicates that the Al/La ratio is 3.08, further confirming that the acicular phase is Al_3La phase. Figure 2d represents BF-TEM image of phases with acicular shape and lamellar shape, and based on the corresponding SAED patterns (Fig. 2e, f), both the acicular and lamellar phases are confirmed as Al_3La phase. It should be noted that the similar phases with acicular or lamellar morphologies are commonly identified as $Al_{11}RE_3$ phase in previously reported Mg–Al–RE-based alloys [13, 14, 22]. This new Al_3La phase has also been confirmed in ALaM440 alloy in our recently work [25], which has monoclinic structure and cell parameters of $a = 0.4437$ nm, $b = 0.4508$ nm, $c = 0.9772$ nm and $\beta = 103.5°$. BF-TEM image of the irregular block phase (inside the yellow dashed box) is shown in Fig. 3a. The corresponding SAED pattern (Fig. 3b) and EDS analysis result (Fig. 3c) show that the irregular block particles are $(Mg,Al)_2Ca$ phase ($a = 0.594$ nm, and $c = 1.971$ nm) with a dihexagonal C36 crystal structure [26, 27].

Figure 4 shows XRD pattern of the as-cast sample. The diffraction peaks of Mg, Al_3La and $(Mg,Al)_2Ca$ phases are identified from XRD pattern, while other diffraction peaks for Al-RE phases such as $Al_{11}La_3$ or Al_2La are not found, further confirming that the acicular/lamellar phase is Al_3La but not $Al_{11}La_3$ phase in the studied alloy.

3.2 Microstructure of peak-aged ALaX431 alloy

The HPDC ALaX431 alloy reaches the peak yield strength when aged at 200 °C for 144 h; hereafter, the sample aged at 200 °C for 144 h is denominated as peak-aged sample.

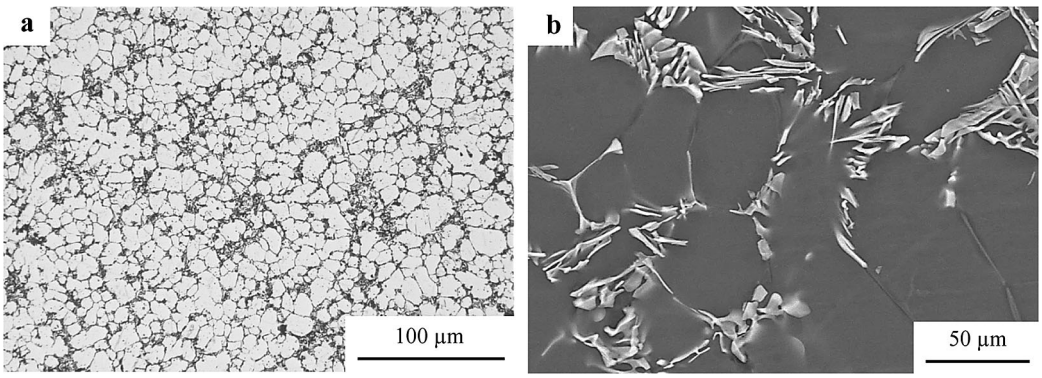

Fig. 1 **a** OM image and **b** SEM image of as-cast ALaX431 sample

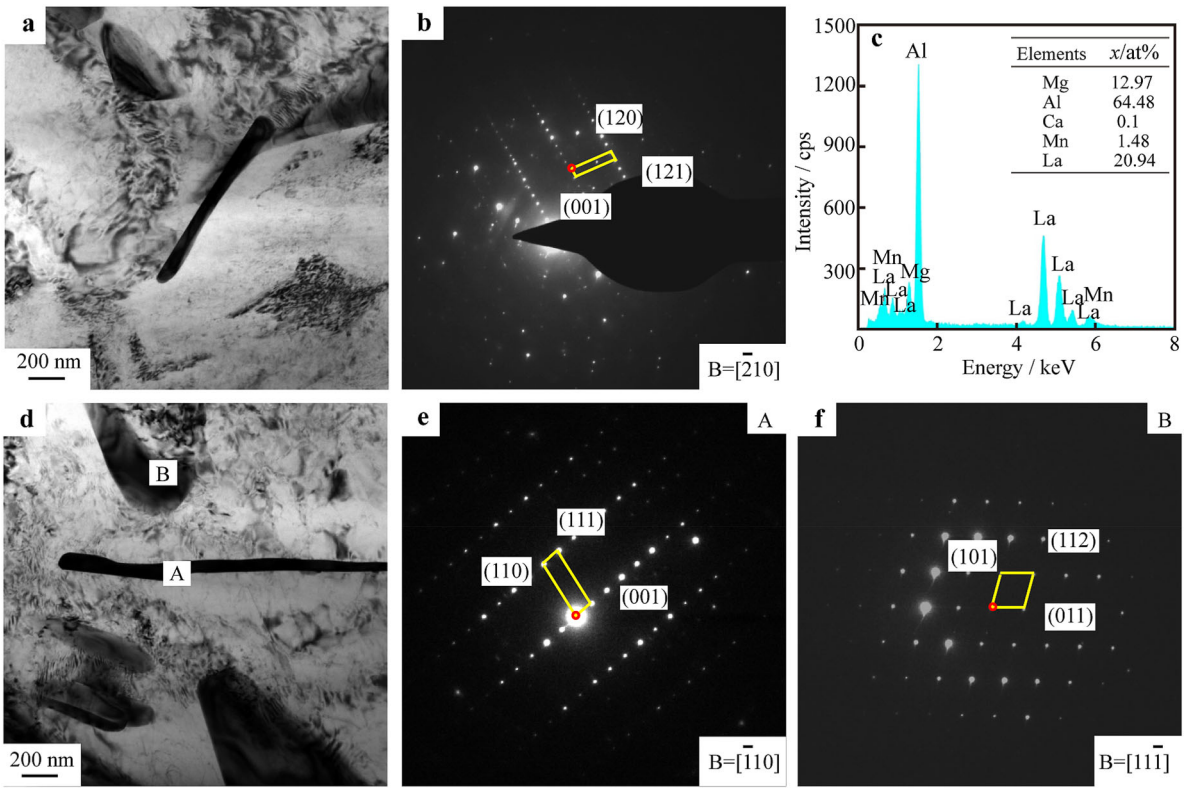

Fig. 2 **a** BF-TEM image, **b** corresponding SAED pattern and **c** EDS result for acicular phase; **d** BF-TEM image showing phases with acicular shape and lamellar shape and **e**, **f** corresponding SAED patterns from local regions indicated by A and B in **d**

The OM and backscatter SEM images of the peak-aged alloy are shown in Fig. 5. The average grain size is measured to be (8.7 ± 0.3) μm, indicating that the grain size of studied alloy is almost unchanged, and the grain boundaries are stable after peak aging treatment. Moreover, it can be seen that the morphology and distribution of intermetallic phases have no discernible changes after peak aging treatment.

The microstructure of peak-aged sample was further characterized by TEM to try to find out the microstructure features and changes. The acicular/lamellar particles, like those in the as-cast sample, are still Al_3La phase based on analysis of BF-TEM images and corresponding SAED patterns (Fig. 6a–c). The irregular particle connected with Al_3La phase is determined as $(Mg,Al)_2Ca$ phase as that in as-cast sample, based on the corresponding SAED pattern and TEM-EDS mappings (Fig. 6b, d–j). In addition, the fine elliptic phase is observed on side of the Al_3La phase from the high resolution TEM (HRTEM) image (Fig. 6a), which is not found in the as-cast sample, and corresponding fast Fourier transform (FFT) pattern (Fig. 6c) suggests that the elliptical phase is Al_6Mn, and it follows an orientation

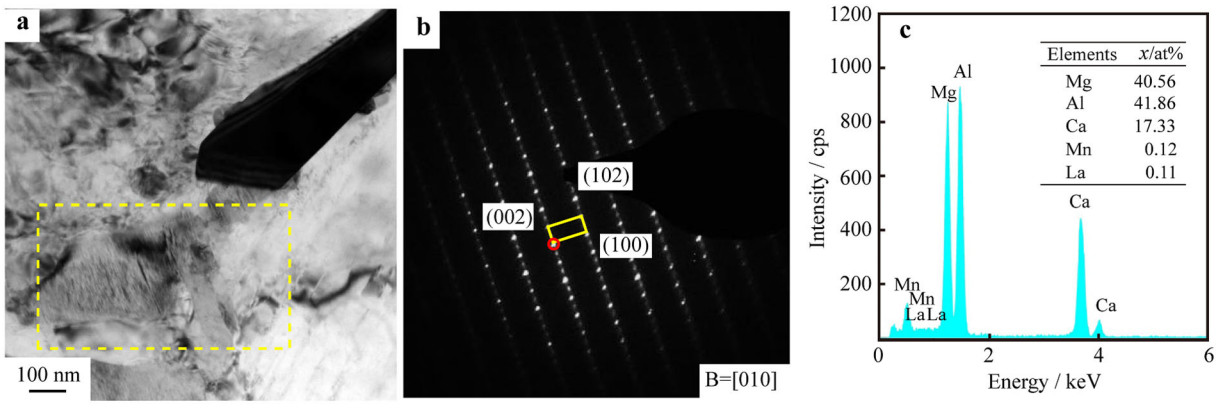

Fig. 3 **a** BF-TEM image, **b** corresponding SAED pattern and **c** EDS result for irregular block phase

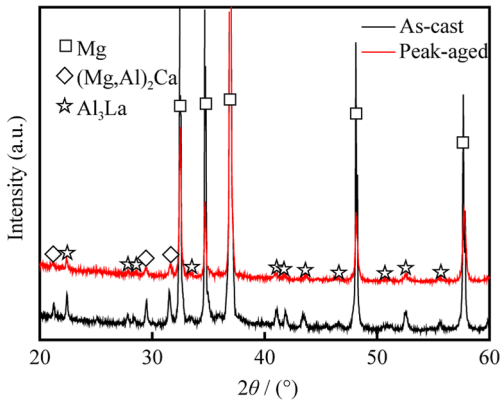

Fig. 4 XRD patterns of as-cast and peak-aged ALaX431 samples

relationship (OR) with Al_3La phase as: $[\bar{1}10]_{Al_6Mn}$// $[100]_{Al_3La}$ and $(111)_{Al_6Mn}$//$(010)_{Al_3La}$. EDS mappings indicate that Mn atoms tend to segregate into the Al_3La phase but not in the $(Mg,Al)_2Ca$ phase (Fig. 6f–j). This may be the reason for the precipitation of fine Al_6Mn particle on the side of Al_3La phase after aging.

Figure 7 presents TEM images, showing the main microstructure changes after peak aging, i.e., aging precipitation. Numerous nanoscale precipitates with different length of 10-60 nm and thickness of 1–2 nm parallel to the (0001) basal plane are observed near grain boundary (Fig. 7a) and within grain (Fig. 7b, c). Although SAED pattern (Fig. 7d) cannot effectively identify the phase structure due to its too small size, it is considered that they are Al_2Ca precipitates (fcc-based C15 structure, a = 0.8022 nm) based on previous reports [28]. It is noted the XRD pattern shown in Fig. 4 also fails to identify the nanometer precipitation. After aging, the diffraction peaks are still for Mg, Al_3La and $(Mg,Al)_2Ca$ as those in the as-cast sample. In addition, careful analysis of XRD shows that the positions of $(Mg,Al)_2Ca$ phase diffraction peaks shifted to higher degrees, indicating a decrease of the lattice parameters of $(Mg,Al)_2Ca$ phase. The calculation based on HRTEM analysis indicates the lattice parameters of a and c for $(Mg,Al)_2Ca$ are 1.971 and 0.594 nm in as-cast sample and 1.877 and 0.569 nm in peak-aged sample, which is consistent with the XRD results. The relevant mechanism needs further study.

3.3 Mechanical properties

Figure 8a shows the aging response of tensile yield strength (TYS) for HPDC ALaX431 alloy at 200 °C up to

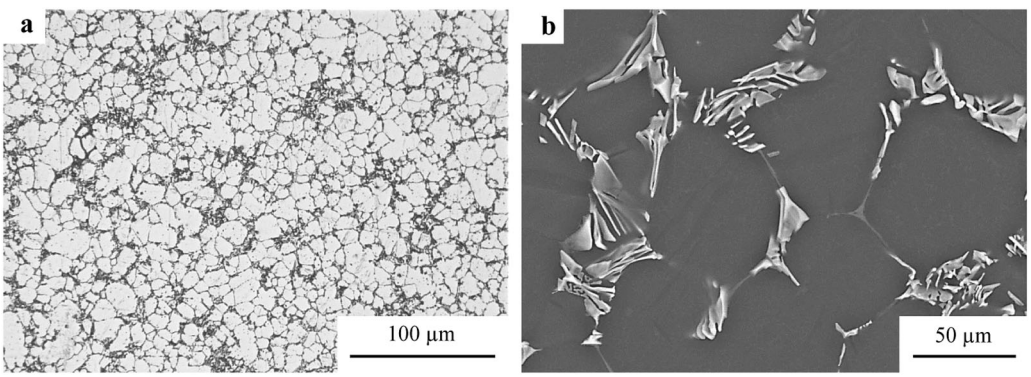

Fig. 5 **a** OM image and **b** SEM image of peak-aged ALaX431 sample

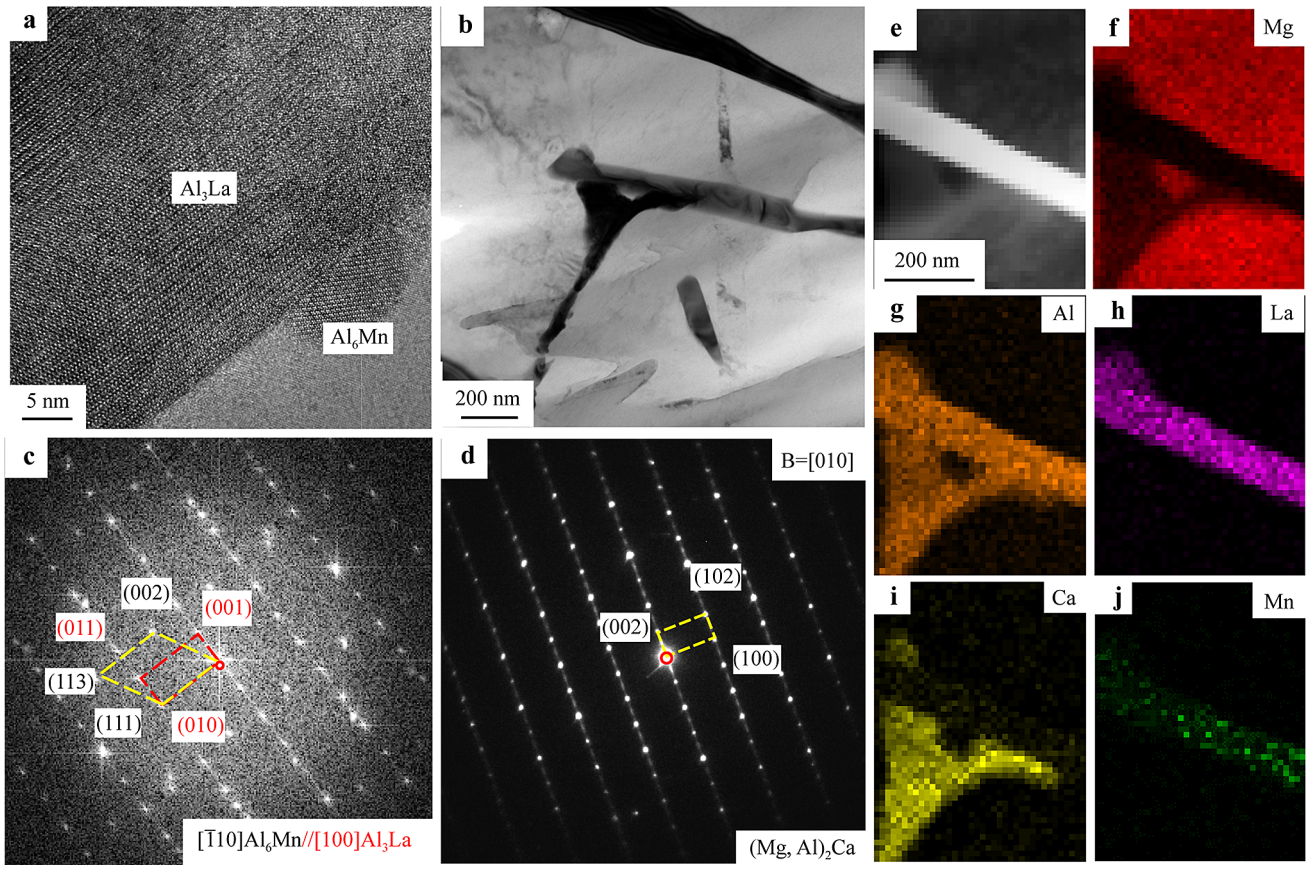

Fig. 6 **a** HRTEM image of lamellar phase and elliptical phase along with **c** corresponding FFT; **b** BF-TEM image of irregular phase and **d** corresponding SAED pattern; **e** high-angle annular dark-field scanning TEM (HAADF-STEM) image along with **f–j** EDS mappings

168 h. The new HPDC alloy exhibits remarkable age strengthening response (ΔTYS = 42 MPa). The TYS of as-cast sample is 178 MPa, and the peak TYS value of 220 MPa is obtained at ~ 144 h. After peak aging, the TYS decreases slowly. It is also implied that peak-aged alloy is not suitable for prolonged use at high temperatures such as 200 °C in order to maintain a high TYS of 220 MPa at RT. This study demonstrates that some HPDC alloy can also be strengthened by aging, and the newly designed ALaX431 HPDC alloy has obvious age strengthening effect. Figure 8b shows the representative tensile strain–stress curves for both as-cast and peak-aged ALaX431 samples at RT (20 °C), 150, 200 and 250 °C. The tensile properties including ultimate tensile strength (UTS), TYS and elongation to failure (ε) of the present ALaX431 alloy and recently reported HPDC Mg alloys are summarized in Table 1 [1, 11, 13, 16, 23, 29–31]. The as-cast sample exhibits excellent combination of strength and ductility regardless of RT or high temperatures up to 250 °C. After aging, the TYS of peak-aged alloy is further improved obviously at RT or high temperatures, and the ductility remains at an acceptable level (6.3% at RT) despite some decrease. Through extensive comparison, it is found that the TYS of new HPDC ALaX431 alloy at peak-aged state is highest of all the reported HPDC Mg alloys at RT and high temperatures as far as the authors are aware. Compared with the commercial HPDC AE44 alloy, the TYS (220 MPa) of the new alloy in peak-aged state at RT is 72 MPa higher than that of the AE44 alloy (148 MPa), and the TYS of 145 MPa at 250 °C is 56 MPa higher than that of the AE44 alloy (89 MPa).

It is considered that the strengthening of HPDC ALaX431 alloy in peak-aged state is at least related to the following factors. Firstly, the ALaX431 alloy owns fine grained structure due to the high cooling rate in HPDC process and the constitutional supercooling of co-addition of La and Ca, providing the effective fine-grain strengthening. By comparison, it is found that the grain size (~ 8–9 μm) of new ALaX431 alloy is smaller than that of most HPDC Mg alloys reported previously, including commercial AE44 alloy (10–20 μm [23]). Secondly, the semi-continuous reticular structure consisting of Al_3La and $(Mg,Al)_2Ca$ particles is formed on grain boundaries of the ALaX431 alloy. The type, size and distribution of intermetallic phases would influence their strengthening effect. It has been reported that the main intermetallic phase Al_3La

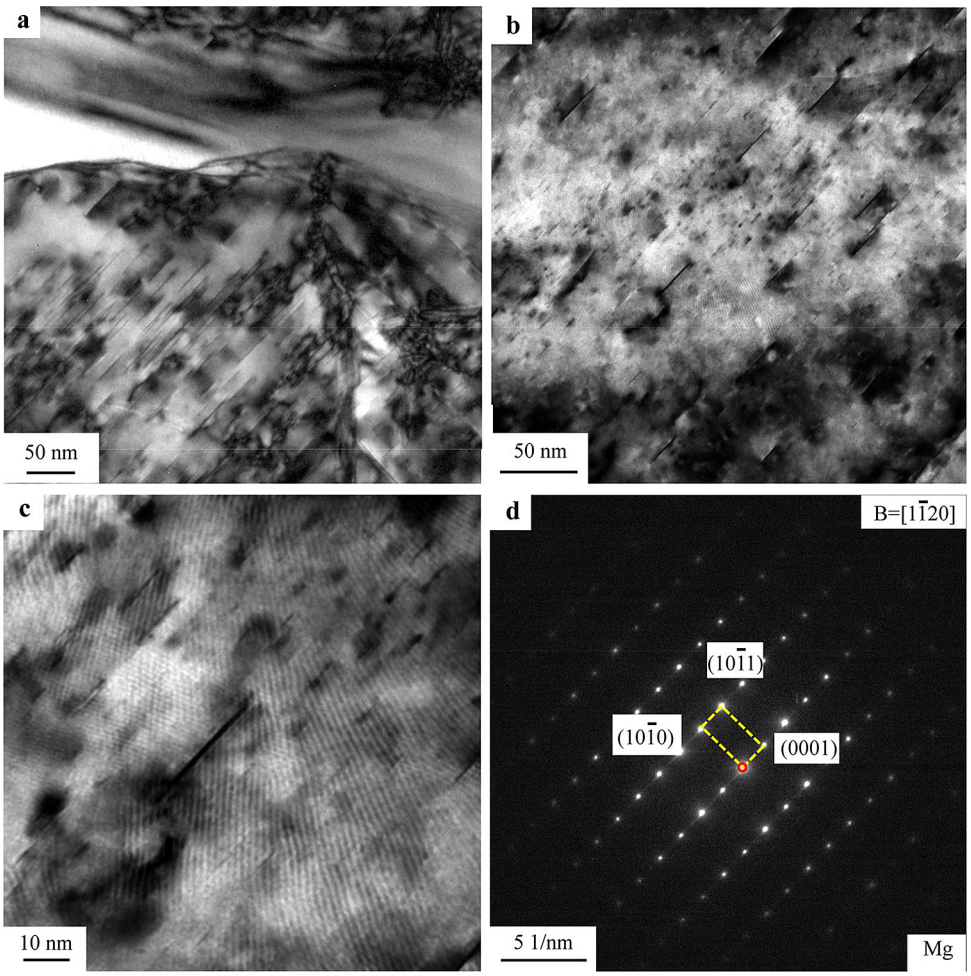

Fig. 7 **a** BF-TEM image showing precipitation near grain boundary; **b–d** BF-TEM images showing precipitates within grain along with corresponding SAED pattern

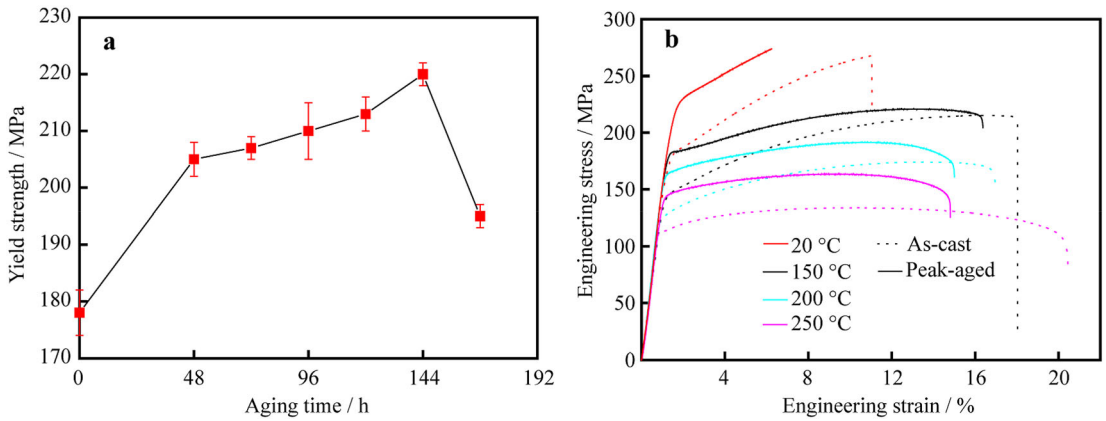

Fig. 8 **a** Variation of TYS as a function of aging time at 200 °C in ALaX431 alloy; **b** representative tensile curves of as-cast and peak-aged samples at different temperatures

in ALaX431 alloy has higher bulk modulus (66.2 GPa) than the C15, C36 phases (< 58 GPa) in AX51 and AX52 alloys [11, 25], and Al_3La phase ordinarily has finer size than the $Al_{11}La_3$ phase in HPDC Mg alloys [25]. Moreover, Al_3La and $(Mg,Al)_2Ca$ phases have the higher melting point than the common intermetallic $Mg_{17}Al_{12}$ phase in Mg–Al bases alloys such as AZ91, and they barely change before and after aging in this study, suggesting the

Table 1 Tensile properties of HPDC ALaX431 alloy and reported HPDC Mg alloys at RT and high temperatures

Alloys	RT			150 °C			200 °C			250 °C		
	UTS/MPa	TYS/MPa	ε/%	UTS/MPa	TYS/MPa	ε/%	UTS/MPa	TYS/MPa	ε/%	UTS/MPa	TYS/MPa	ε/%
As-cast ALaX431	267	178	11	215	143	18	174	127	17	134	113	20
Peak-aged ALaX431	274	220	6.3	220	180	16	191	164	14	163	145	13
AE44 [23, 29]	245	148	11	157	123	23	120	100	24	105	89	16
AX51 [30]	192	128	7	161	102	7						
AX52 [1, 31]	228	161	13									
AEX422 [11]	234	204	4	192	145	6	164	126	17	119	110	29
ALa44 [13]	265	155	12	160	125	25	126	107	24	104	91	15
ANd44 [16]	262	154	13	161	119	17	114	101	14			
AZ91 [30]	239	157	4.7	170	105	18						

relatively high stability of these two intermetallic phases. Therefore, it is considered that the formation of Al_3La and $(Mg,Al)_2Ca$ semi-continuous reticular structure along grain boundaries would contribute to high strength at RT and high temperatures. Thirdly, after peak aging, a large number of nanoscale precipitates are formed in grains of ALaX431 alloy, which is obviously the main reason for the further improved strength of the peak-aged alloy.

4 Conclusion

In this work, a new HPDC Mg–4Al–3La–1Ca–0.3Mn (wt%) alloy was fabricated. Fine grained structure along with the semi-continuous reticular structure consisting of Al_3La and $(Mg,Al)_2Ca$ particles on grain boundaries were formed in ALaX431 alloy due to HPDC process and co-addition of La and Ca. After aging at 200 °C for 144 h, the grain size ($\sim$ 8–9 μm) and original Al_3La and $(Mg,Al)_2Ca$ intermetallics barely change. A few Al_6Mn nano-particles are precipitated next to Al_3La, and the OR between them is: $(111)_{Al_6Mn}//(100)_{Al_3La}$ and $[\bar{1}10]_{Al_6Mn}//[010]_{Al_3La}$. The main microstructural change caused by aging is the formation of numerous nanoscale Al_2Ca precipitates in grains.

The HPDC ALaX431 alloy in peak-aged state reveals the highest TYS among the HPDC Mg alloys reported so far; TYS of 220 MPa at RT and TYS of 145 MPa at 250 °C have been obtained. The high strength is mainly attributed to the formation of fine grained structure with Al_3La and $(Mg,Al)_2Ca$ particles along grain boundaries and nanoscale Al_2Ca precipitates in grains. The new developed HPDC ALaX431 alloy in this work has more excellent mechanical properties and cost performance than the commercial HPDC AE44 alloy, and hence has good application potential.

Acknowledgements This work was financially supported by the National Natural Science Foundation of China (Nos. 51701200 and 11804030), the Fundamental Research Funds for the Central Universities (No. 3072020CF1009), the Open Funds of the State Key Laboratory of Rare Earth Resource Utilization (Nos. RERU2020008 and 2020012), the Scientific and Technological Developing Scheme of Jilin Province (No. 20200801048GH) and the Jilin Scientific and Technological Development Programs (No. 20200201240JC).

References

[1] Pekguleryuz MO, Kaya AA. Creep resistant magnesium alloys for powertrain applications. Adv Eng Mater. 2003;5(12):866.
[2] Pekguleryuz M, Celikin M. Creep resistance in magnesium alloys. Int Mater Rev. 2010;55(4):197.
[3] Yang Q, Lv SH, Qin PF, Qiu X, Hua XR, Guan K, Sun W, Liu XJ, Meng J. Interphase boundary segregation induced phase transformation in a high-pressure die casting Mg–Al–La–-Ca–Mn alloy. Mater Des. 2020;190:108566.
[4] Bakke P, Bowles AL, Westengen H. Elevated temperature alloys—paths for further performance gains in AE44. In: Kainer KU, editors. Magnesium: Proceedings of the 7th International Conference Magnesium Alloys and their Applications. Weinheim: WILEY-VCH Verlag GmbH, 2007. 55.
[5] Lv S, Lü X, Meng F, Yang Q, Qiu X, Qin P, Duan Q, Meng J. Microstructures and mechanical properties in a Gd-modified high-pressure die casting Mg–4Al–3La–0.3Mn alloy. Mater Sci Eng A. 2020;773:138725.
[6] Xu SW, Matsumoto N, Yamamoto K, Kamado S, Honma T, Kojima Y. High temperature tensile properties of as-cast Mg–Al–Ca alloys. Mater Sci Eng A. 2009;509(1–2):105.
[7] Suzuki A, Saddock ND, Terbush JR, Powell BR, Jones JW, Pollock TM. Precipitation strengthening of a Mg–Al–Ca-based AXJ530 die-cast alloy. Metall Mater Trans A. 2008;39(3):696.
[8] Nami B, Razavi H, Miresmaeili SM, Mirdamadi S, Shabestari SG. Impression creep properties of a semi-solid processed magnesium–aluminum alloy containing calcium and rare earth elements. Scr Mater. 2011;65(3):221.
[9] Nami B, Razavi H, Mirdamadi S, Shabestari SG, Miresmaeili SM. Effect of Ca and rare earth elements on impression creep properties of AZ91 magnesium alloy. Metall Mater Trans A. 2010;41(8):1973.

[10] Wang QD, Peng JG, Michel S, Blandin JJ. Effects of aging on the microstructures and mechanical properties of extruded AM50 + xCa magnesium alloys. Rare Met. 2006;25(4):377.
[11] Yang Q, Guan K, Bu FQ, Zhang YQ, Qiu X, Tian Z, Liu XJ, Meng J. Microstructures and tensile properties of a high-strength die-cast Mg–4Al–2RE–2Ca–0.3Mn alloy. Mater Charact. 2016; 113:180.
[12] Zhang Y, Yang L, Dai J, Guo G, Liu Z. Effect of Ca and Sr on microstructure and compressive creep property of Mg–4Al–RE alloys. Mater Sci Eng A. 2014;610:309.
[13] Zhang JH, Zhang ML, Meng J, Wu RZ, Tang DX. Microstructures and mechanical properties of heat-resistant high-pressure die-cast Mg–4Al–xLa–0.3Mn (x = 1, 2, 4, 6) alloys. Mater Sci Eng A. 2010;527(10–11):2527.
[14] Zhang JH, Leng Z, Zhang ML, Meng J, Wu RZ. Effect of Ce on microstructure, mechanical properties and corrosion behavior of high-pressure die-cast Mg–4Al-based alloy. J Alloys Compd. 2011;509(3):1069.
[15] Wu HR, Du WB, Li SB, Liu K, Wang ZH. Microstructure and mechanical properties of AZ31 magnesium alloy reinforced by I-phase. Rare Met. 2019;38(8):733.
[16] Su ML, Zhang JH, Feng Y, Bai YJ, Wang W, Zhang ZW, Jiang FC. Al–Nd intermetallic phase stability and its effects on mechanical properties and corrosion resistance of HPDC Mg–4Al–4Nd–0.2Mn alloy. J Alloys Compd. 2017;691:634.
[17] Tian Z, Yang Q, Guan K, Cao ZY, Meng J. Microstructural evolution and aging behavior of Mg–4.5Y–2.5Nd–1.0Gd–0.5Zr alloys with different Zn additions. Rare Met. 2020. https://doi.org/10.1007/s12598-020-01510-5.
[18] Zhang Z, Zhang JH, Wang J, Li ZH, Xie JS, Liu SJ, Guan K, Wu RZ. Toward the development of Mg alloys with simultaneously improved strength and ductility by refining grain size via the deformation process. Int J Miner Metall Mater. 2020. https://doi.org/10.1007/s12613-020-2190-1.
[19] Qin PF, Yang Q, Guan K, Meng FZ, Lv SH, Li BS, Zhang DD, Wang N, Zhang JH, Meng J. Microstructures and mechanical properties of a high pressure die-cast Mg–4Al–4Gd–0.3Mn alloy. Mater Sci Eng A. 2019;764:138254.
[20] Guan K, Meng FZ, Qin PF, Yang Q, Zhang DD, Li BS, Sun W, Lv SH, Huang YD, Hort N, Meng J. Effects of samarium content on microstructure and mechanical properties of Mg–0.5Zn–0.5Zr alloy. J Mater Sci Technol. 2019;35(7):1368.
[21] Anyanwu IA, Gokan Y, Suzuki A, Kamado S, Kojima Y, Takeda S, Ishida T. Effect of substituting cerium-rich mischmetal with lanthanum on high temperature properties of die-cast Mg–Zn–Al–Ca–RE alloys. Mater Sci Eng A. 2004; 380(1–2):93.
[22] Zhu SM, Easton MA, Abbott TB, Gibson MA, Nie JF. The influence of individual rare earth elements (La, Ce, or Nd) on creep resistance of die-cast magnesium alloy AE44. Adv Eng Mater. 2012;18(6):932.
[23] Zhang J, Yu P, Liu K, Fang D, Tang D, Meng J. Effect of substituting cerium-rich mischmetal with lanthanum on microstructure and mechanical properties of die-cast Mg–Al–RE alloys. Mater Des. 2009;30(7):2372.
[24] Luo AA, Balogh MP, Powell BR. Creep and microstructure of magnesium–aluminum–calcium based alloys. Metall Mater Trans A. 2002;33(3):567.
[25] Meng FZ, Lv SH, Yang Q, Qin PF, Zhang JH, Guan K, Huang YD, Hort N, Li BS, Liu XJ, Meng J. Developing a die casting magnesium alloy with excellent mechanical performance by controlling intermetallic phase. J Alloys Compd. 2019;795:436.
[26] Suzuki A, Saddock ND, Jones JW, Pollock TM. Structure and transition of eutectic (Mg, Al)$_2$Ca Laves phase in a die-cast Mg–Al–Ca base alloy. Scr Mater. 2004;51(10):1005.
[27] Zhu SM, Mordike BL, Nie JF. Creep and rupture properties of a squeeze-cast Mg–Al–Ca alloy. Metall Mater Trans A. 2006; 37(4):1221.
[28] Liu XQ, Qiao XG, Li Z, Zheng MY. High strength and excellent ductility of dilute Mg–0.68Al–0.32Ca–0.50Mn (wt%) extrusion alloy obtained by T6 treatment. Mater Charact. 2020;162:110197.
[29] Zhang JH, Liu SJ, Leng Z, Zhang ML, Meng J, Wu RZ. Microstructures and mechanical properties of heat-resistant HPDC Mg–4Al-based alloys containing cheap mischmetal. Mater Sci Eng A. 2011;528(6):2670.
[30] Luo AA. Recent magnesium alloy development for elevated temperature applications. Int Mater Rev. 2004;49(1):13.
[31] Pekguleryuz MO. Magnesium diecasting alloys for high temperature applications. In: Luo AA, editors. Magnesium Technology 2004. TMS 2004. 281.